

Rapid and step-wise eye growth in molting diving beetle larvae

Shannon Werner¹ · Elke K. Buschbeck¹

Received: 13 June 2015 / Revised: 19 August 2015 / Accepted: 26 August 2015 / Published online: 10 September 2015
© Springer-Verlag Berlin Heidelberg 2015

Abstract However complex a visual system is, the size (and growth rate) of all its components—lens, retina and nervous system—must be precisely tuned to each other for the system to be functional. As organisms grow, their eyes must be able to achieve and maintain emmetropia, a state in which photoreceptors receive sharp images of objects that are at infinity. While there has been ample research into how vertebrates coordinate eyes growth, this has never been addressed in arthropods with camera eyes, which tend to grow dramatically and typically in a step-wise manner with each molt (ecdysis). Here, we used histological and optical methods to measure how the larval eyes of Sunburst Diving Beetles (*Thermonectus marmoratus*, Coleoptera, Dytiscidae) grow, and how well optical and morphological parameters match, during the dramatic growth that occurs between two consecutive larval stages. We find that the eye tubes of the principal eyes of *T. marmoratus* grow substantially around molt, with the vitreous-like crystalline cone contributing the most to the overall growth. Lenses also reform relatively quickly, undergoing a period of dysfunction and then regaining the ability to project sharp images onto the retina around 8 h post-molt.

Keywords Emmetropia · Eye growth · Arthropod · Vision · Stemmata

Introduction

Eyes have long been known to be among the most complex and intricate organs. Even Charles Darwin specifically pondered about their evolutionary origins as he recognized them as “organs of extreme perfection and complication” (Darwin 1859). Eye development requires that essential properties (such as size and transparency) of many different tissues are extremely tightly coordinated, especially while undergoing substantial growth. In addition, coordination needs to be maintained long term to allow eyes to stay functional. In vertebrates, eye growth has been an important topic of active research (for reviews see McBrien and Barnes 1984; Wallman and Winawer 2004; Flitcroft 2013). However, vertebrates are not the only organisms with sophisticated image-forming eyes (Land and Nilsson 2012). Many invertebrates including spiders (Land 1969, 1985) and holometabolous insect larvae (Gilbert 1994; Buschbeck 2014) also have camera-type image-forming eyes that undergo substantial growth during their lifetime and thus necessarily must have mechanisms that tightly control eye growth. However, thus far it has been essentially unstudied how growth in invertebrate eyes is coordinated to allow optimal focusing.

Most vertebrate eyes are emmetropic, which means that, in the relaxed eye, images of objects at infinity are in sharp focus on the retina. In many such vertebrate eyes, near objects are then brought into focus through accommodation. At birth, the camera-type eyes of vertebrates typically are, depending on the species, either hyperopic (far-sighted, refractive power is too low to focus on the retina) or myopic (near-sighted, refractive power is too high to focus on the retina; Wallman and Winawer 2004), but gain emmetropia during development (Hofstetter 1969). Over the course

✉ Elke K. Buschbeck
elke.buschbeck@uc.edu

¹ Department of Biological Sciences, University of Cincinnati, Cincinnati, OH 45221-0006, USA

of many studies, it has become clear that eye growth is a highly complex process contributed to by passive means, stochastic events and homeostatic feedback (Troilo 1992; Flitcroft 2014). Passive regulation includes physical characteristics that allow them to “automatically” grow towards emmetropia (Mark 1972) and eye-growth models that are based on physical parameters favor a reduction in refractive errors as eyes get larger (Hofstetter 1969). There also is strong evidence for homeostatic feedback, which consists of both the kind of feedback that is typical for the development of other organs (Wallman and Winawer 2004) and of visual feedback (Troilo and Wallman 1991; Flitcroft 2013). The importance of the latter has been demonstrated in many vertebrates, including in fish (Kroger and Wagner

1996), chicks (Schaeffel et al. 1988), guinea pigs (McFadden et al. 2004), and primates (Hung et al. 1995). While eye growth is extensively studied in vertebrates, we know little about how eyes grow in invertebrates, despite their diversity of interesting eye organizations.

One example of particularly sophisticated image-forming eyes is the principal eyes of diving beetle (*T. marmoratus*) larvae. These eyes are large and tubular, look directly forward (Fig. 1a), and are important for visually guided prey capture (Buschbeck et al. 2007). Each eye has a retina that is divided into a distinct green-sensitive distal (DR) and ultraviolet and polarization sensitive proximal (PR) portion (Fig. 1b; Mandapaka et al. 2006; Maksimovic et al. 2009). Functionally these eyes stand out for the presence

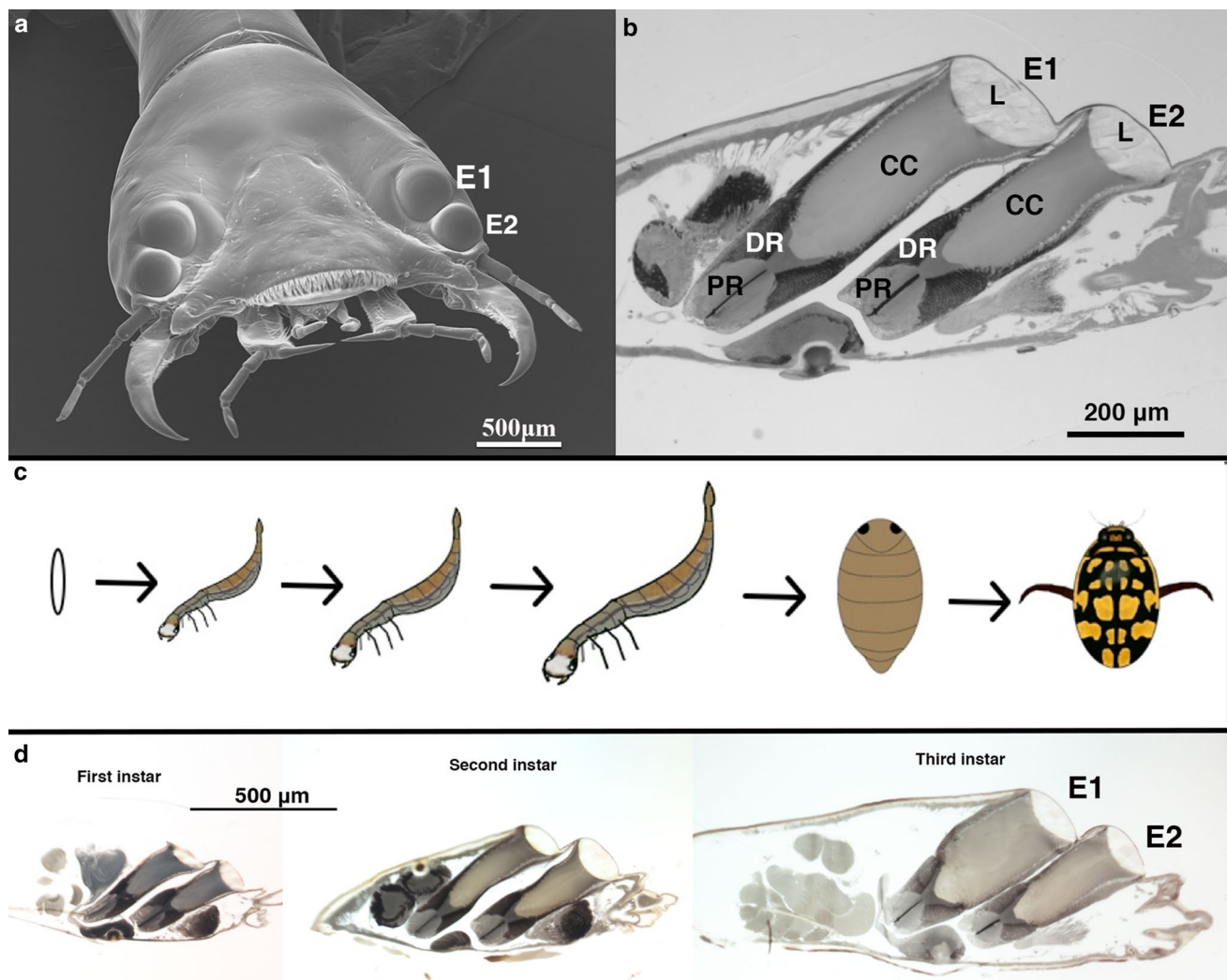


Fig. 1 Visual system and development of *Thermonectus marmoratus* larvae. **a** An electron microscopy image of the whole larval head, illustrating the position of the two main eyes, eye1 (E1) and eye2 (E2). **b** Sagittal section of the larval eyes showing important anatomical structures within each of the main eyes. L lens, CC crystal

cone, DR distal retina, PR proximal retina. **c** Diagram of the life cycle of *T. marmoratus*, from egg to adulthood, illustrating dramatic growth between some of the stages (which are drawn to scale). **d** Sagittal sections through the eye tubes of larvae from three different developmental states illustrate eye growth between these stages

of bifocal lenses (Stowasser et al. 2010) that are organized so that, during prey approach, images maximally excite specific regions, with eye 1 being optimized for relatively close objects, and eye 2 for further objects (Stowasser and Buschbeck 2014). *Thermonectus marmoratus* has three larval instars (Fig. 1c) all of which are predatory, relying on good vision to accommodate their predatory life style, but differ substantially in size. First instars are approximately 1 cm long, whereas second instars are around 1.7 cm and third instars (around 2.5 cm) are more than twice the length of first instars. While vertebrates and their eyes grow gradually, arthropod eye growth may be constrained by the step-wise enlargement of their exoskeleton that accompanies each molt. Based on initial histological observations (Fig. 1d), their eyes grow substantially with each larval instar, and observations in our laboratory (Werner 2014) suggest that larvae already are able to hunt mosquitoes on the first day after molting, but maximize prey capture activities around the third day. It remains unclear though, if changes in eye size co-occur with the step-wise dramatic change in body size during ecdysis, or if eye growth occurs more gradually. Therefore, it is subject to the current investigation how and when eye growth occurs. To address this question, we performed histological and optical measurements through a range of developmental stages. Specifically, we focused on the second molt that gives rise to the third and final larval stage of *T. marmoratus*. We investigated the size of the eyes and their key components as well as the optical power of their lenses from 3 days prior to their expected molting time, to 2 days post-molt. To the best of our knowledge, this kind of question has never before been addressed in arthropods, though one study that used MicroCT imaging in spiders suggests that arthropod lenses can undergo some changes following ecdysis (Fenk et al. 2010). Our data suggest that *Thermonectus* eye growth co-occurs extremely rapidly with overall change in body size during ecdysis.

Materials and methods

Animal rearing, surveillance and sampling

Thermonectus marmoratus larvae were offspring of beetles from our colony, which is derived from wild stock originally collected in the vicinity of Tucson, AZ, USA, or were provided by the Cincinnati Zoo and Botanical garden. To minimize variation, larvae derived from large egg clutches that were reared simultaneously in a dedicated incubator and with standardized nutritional supply (consisting of mosquito larvae and bloodworms). To accurately observe individual molt times, and determine the sampling schedule for each individual, larvae were video monitored

around the clock. To do so, the incubator was equipped with a stand-alone fluorescent fixture for day lighting, and two infrared LED arrays during dark cycles. Images were captured every 15 min with a Microsoft Life Cam Studio 1080p, modified for light and infrared capture by removal of the infrared cut-off filter. High-resolution time-lapse images were evaluated in regard to occurrence of molting. To minimize bias, clutches were maximally spread over different samples, with no more than two individuals of a clutch contributing to individual sample times.

As a first step towards measuring optical and histological parameters pre- and post-molting, we first established how fast larvae developed under consistent rearing conditions. In those trials, we noted that at 24 °C with a cycle of 14-h light and 10-h dark, the second instar phase lasted 5 days in 86 % of our trials, with a few animals molting slightly earlier or later. The third instar phase typically lasted 6 days. Optical and histological data were collected from day three of second instars and continued to 48 h post-molt in third instars. Samples were taken daily, except for the first 24 h post-molt, during which samples were taken every 4 h, since we anticipated most changes during that time window. An additional sample was also taken at 36 h. The first post-molt sample (labeled “molt” on all graphs) was taken as quickly as possible after molting was detected, in all cases within a time window of 60 min.

For each sample, larvae were first anesthetized on ice, decapitated, and the head photographed against a scale to establish a record of its size, which later was used to normalize data. Thereafter, the head was bisected, using its left half for histology and its right half for lens optics measurements following methods described by Stowasser et al. (2010) and Stowasser and Buschbeck (2014).

Histology processing and size measurements

The left side of head capsules was fixed for 2 h (at room temperature) or up to 24 h (at 4 °C) in a solution of 2 % glutaraldehyde (Electron Microscopy Sciences) in Sørensen's phosphate buffer at pH 7.4 (Electron Microscopy Sciences). After fixation, tissue was washed and post-fixed (1 h on ice followed by 1 h at room temperature) in 1 % OsO₄ solution (Electron Microscopy Sciences). Thereafter, the tissue was thoroughly washed in water, dehydrated through a graded series of alcohol and acetone, and embedded in Ultra-Low Viscosity Embedding Medium (Electron Microscopy Sciences). Finally, tissue was sectioned sagittally at 6–7 μm and mounted on slides. Histological sections were imaged through a microscope with a digital camera and the dimension of key components was established in ImageJ using pixel sizes. To ensure consistency in these measurements, only central sections of each eye were chosen, and other parameters (such as the presence of eye

5 in that section) were consistently met. To minimize sampling errors, five measurements were taken for each eye.

For each of the two principal eyes and for each time point, we determined the following parameters (Fig. 1b): the length of the entire eye (from the back of the lens to its fullest extent), the length of the crystalline cone (a vitreous-like structure that separates the back of the lens from the two retinas) and the overall thickness of each of the two retinas. Data for each sample point derived from at least 5 (but up to 12) independent preparations. Histological data were compiled in Excel, where pixel values were converted to microns based on images of scales. To compensate for general size variation, data of each age class were normalized based on the head size, and all histological data were corrected for 6 % shrinkage (as established in Stowasser and Buschbeck 2014). Finally, all samples were assessed by ANOVA and pairs were compared with a Tukey Test in JMP (JMP 9.0.1).

Optical imaging and image contrast measurement

To determine optical parameters, the right half of the head capsule was analyzed using imaging methods previously established in our lab (Stowasser et al. 2010). Specifically, the lenses of the two primary eyes and some of the surrounding exoskeleton were excised from the head capsule and residual tissue was gently removed with forceps and a small brush. Lenses were then placed on an 800- μm diameter pinhole (Edmund Optics) and secured by waxing surrounding cuticle to the metal surrounding the pinhole. Since *Thermonectus* larvae are aquatic, measurements were performed with fully submerged lenses by mounting the pinhole onto a wax ring that was sandwiched between two glass cover slips, and filled with a solution of 50 % insect ringer (Oshea and Adams 1981). This insect ringer concentration appears optimal in regard to preserving the integrity of these lenses (Stowasser et al. 2010). The coverslip stack was then placed back surface up on a goniometer-microscope stage (which was used to correct minor misalignments of lenses), and imaged through a microscope for which the condenser had been removed so that an object could be placed at ~ 12.5 cm distance, which is at effective infinity for these small insect lenses. This object was illuminated with monochromatic green light that was produced by placing a green filter (with a peak transmission of 542 nm) and diffuser plate in front of a fiber optic light illuminator. The object consisted of a square-wave grating (0.353 cycles/mm, USAF 1951 negative test target from Edmund Optics) which was imaged through the insect's lenses. To establish if and how individual lenses produced images, image series were acquired with a high-resolution camera (Moticam 3.0) and time-lapse software (Motic Images Plus 2.0.25). To determine how far images were

produced from the lens, an initial image series (without an object) was taken from the approximate front surface of the insect past its back surface. Thereafter, the object was added, and additional images were taken (at equal sample intervals and known microscope stage positions) from well before to well after the focal planes of each lens. These image stacks were then analyzed with a custom-made Matlab script (Matlab 2014, The Mathworks, Natick, MA) to evaluate which of the images (of the object) resulted in highest edge sharpness (and hence indicated the position of the highest quality images). Image stacks that indicated lens damage or improperly positioning were excluded from further analysis, which included distance correction by a factor of 1.33 (to account for the refractive index of the ringer solution). Sample sizes were: $n = 3$ for +20 h; $n = 4$ for +16 h, +24 h and +48 h; $n = 5$ for -72 h, +8 h, +12 h and +36 h and $n = 8$ for -48 h and -24 h.

Results

For an eye to function optimally, there has to be a tight match between the position of images that are produced by the lens, and the location of the retina. As the eye grows, one expects that the relative position of these parameters is maintained. To determine if that indeed is the case and when and how growth occurs in the principal eyes of *T. marmoratus*, we contrasted selected focal planes with selected anatomical features, as established by Stowasser and Buschbeck (2014). To investigate physical eye growth we used histological preparations to evaluate the size of the eye and its main components before, during, and after the transition to their third instar phase. To evaluate if lenses were able to form sharp images, and to measure their focal lengths at corresponding developmental points, we used a modified hanging drop technique, in which lenses were fully suspended in solution as outlined in Stowasser et al. (2010). To optimally match histology and optics, heads were bisected and the majority of our results are from preparations where the same head was used for both histological and optical methods.

Morphological changes in the eye tube

For each eye, we evaluated the total length of the eye tube, the length of the crystalline cone, and the thickness of each of the two retinas from 3 days pre-molt to 2 days post-molt (Fig. 2). Most notably, for both eyes, eye tube length remained relatively unchanged within instar stages. However, dramatic growth occurred during the transition between the second and third instars stages. The majority of growth was accounted for by an enlargement of the tissue between the lens and the retina, which co-occurred

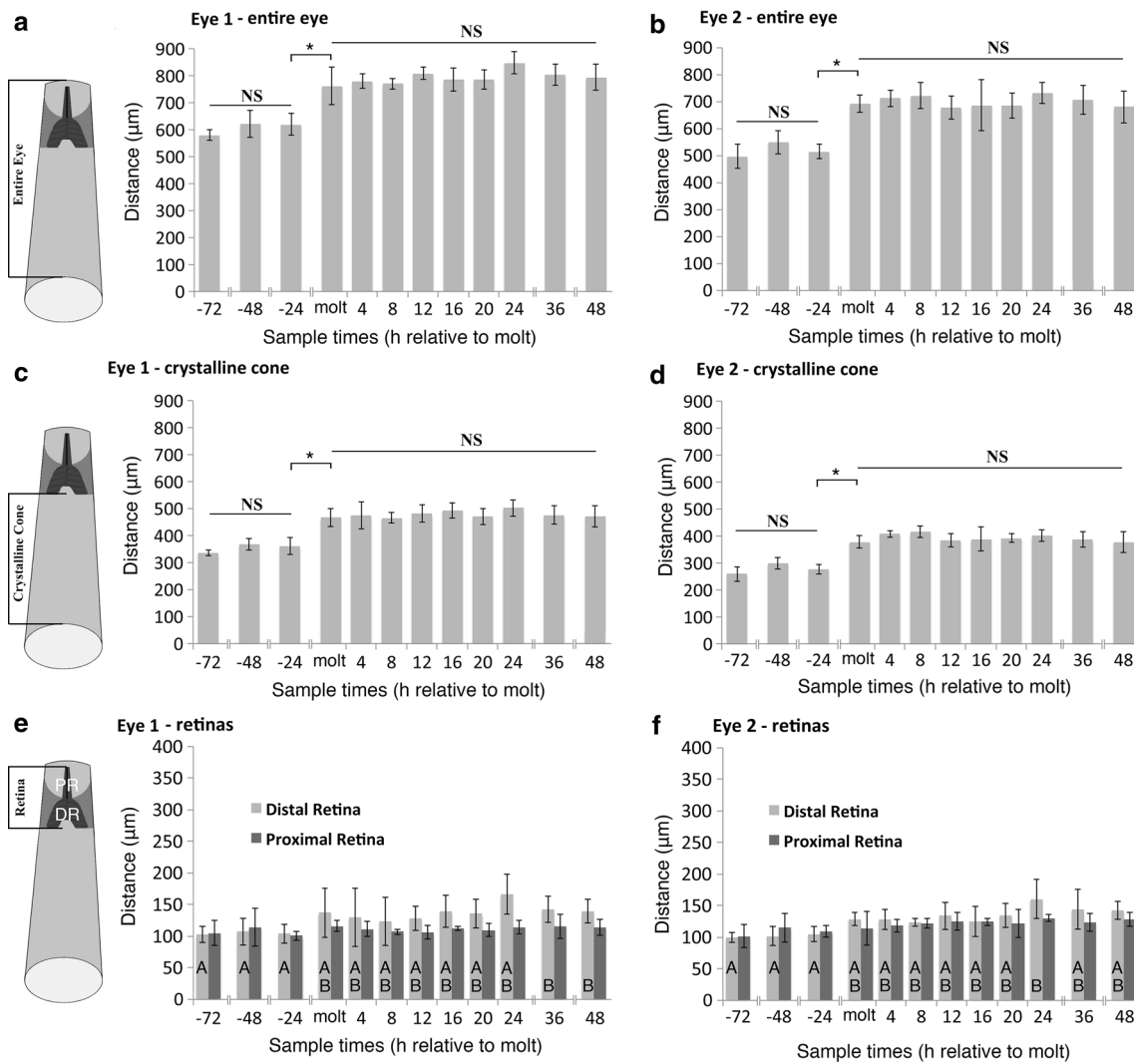


Fig. 2 Average eye growth (with standard deviation) through the transition between second and third instar larvae. **a, b** Histological measurements of the eye length (from behind the lens to the end of the eye as indicated in the schematic to the left) from 3 days prior to the predicted molting time (−72 h) to 2 days post-molt (48 h) show that the eye tube grows rapidly and dramatically at the transition between second and third instar stages. **c, d** The majority of this dramatic growth takes place in the crystalline cone, a spacing tissue

(similar to our vitreous) that is located between the back of the lens and the distal retina as indicated in the schematic to the left. **e, f** Substantial growth also occurs in the distal retina, the position of which is indicated in the schematic to the left. This growth is substantial in the distal retina, where statistical analysis identified overlapping groups A and B. In contrast, insignificant growth was observed in the proximal retina

with ecdysis. In comparison, the retinas, especially the proximal retina, grew relatively less, and its growth may be less tightly linked to the molting period.

Eye 1

In eye one the most dramatic growth of the entire eye and crystalline cone occurred between the last second instar sample, and the first post-molt sample. The eye tubes of eye one (Fig. 2a) grew from an average of 619 µm on the last second instar sampling point (−24 h) to 761 µm at the earliest post-molt sample, a change of 97 µm or 16 %. Most of this growth

was due to the enlargement of the crystalline cone as this region grew from on average of 360 µm at the end of the second instar, to an average of 466 µm at the earliest post-molt time (29 %). An ANOVA and further post hoc Tukey tests showed that there was no significant difference between the crystalline cone lengths within all second instar points (−72, −48, −24), nor between crystalline cone lengths within all third instar points (molt to 48). However, all third instar crystalline cone lengths were significantly longer than all second instar crystalline cones ($P \leq 0.0001$ for all comparisons; Fig. 2c). The growth pattern of the retinas (Fig. 2e) is less clear and it is possible that this area changes more gradually.

Specifically, the ANOVA results ($P = 0.0001$) and further post hoc Tukey HSD test for the thickness of the distal retina showed that there was some growth in that area and that there are significant differences between some of the time points. However, the groups (indicated as A and B in Fig. 2e) overlap and are not tightly linked with molting. Still the distal retina grew from 105 to 129 μm , lengthening by 24 μm (23 %) between the last second and first third instar time points. ANOVA results for the proximal retina showed that there is no significant difference between any of the groups, and it only changed from 109 to 114 μm between the last second and first third instar stages, a change of 5 μm or 4 %.

Eye 2

As in eye one, the most dramatic growth of the entire eye and crystalline cone occurred between the last second instar sample, and the first post-molt sample. The eye tubes of eye two (Fig. 2b) grew from an average of 516 μm on the last second instar sampling point (–24 h) to 693 μm at the earliest post-molt sample, a change of 177 μm or 34 %. In eye two (Fig. 2d), the crystalline cone grew from 278 μm on second instar day five to 379 μm immediately after molt, a change of 101 μm or 36 %. ANOVA results for the eye two crystalline cone region ($P < 0.0001$) demonstrate that there were significant differences between some of the sampled points. Based on post hoc Tukey tests, there was no significant difference in crystalline cone length within the second and third instar points, but all third instar crystalline cone lengths differed significantly from all second instar crystalline cone lengths ($P \leq 0.0001$, Fig. 2d). The retinas (Fig. 2f) of eye 2 also grew less clearly step-wise throughout the developmental stages. The ANOVA results ($P < 0.0012$) and further post hoc Tukey HSD test for the thickness of the distal retina showed that there was some growth in that area and that there were significant differences between some of the time points. However, the groups (identified by the statistical analysis and indicated as A and B in Fig. 2f) overlap and are not tightly linked with molting. In Eye 2, the distal retina grew from 104 to 137 μm , lengthening by 33 μm (32 %) between the last second and first third instar time points. ANOVA results for the proximal retina showed that for this eye as well there was no significant difference between any of the groups, and it only changed from 101 to 116 μm between the last second and first third instar stages, a change of 15 μm or 15 %.

Changes in the lens system

To evaluate optical parameters, insect lenses were isolated and pictures were taken and evaluated; first of the back surface of the lens, and then of images that were produced by that lens (see “Materials and methods”). Figure 3a illustrates an example of the back surface of eye 1 of a

second instar larva. At this stage, lenses appear smooth with no sign of degradation even on the final day of this live stage. Correspondingly, such lenses are capable of forming good, high-contrast bifocal images with two distinct focal planes (Fig. 3d, e, blue lines). Upon ecdysis, a portion of the lens is shed with the exoskeleton, leaving behind a relatively thin section of remaining lens tissue with a distinctly rough surface (Fig. 3b). Interestingly, very early post-molt (sampled within 4 h after molting) lenses are not capable of forming images, and image processing at these time points results in consistently low image contrast scores (red lines, Fig. 3d, e). The lenses of older third instar larvae (Fig. 3c) appear to have smooth back surfaces again and are of larger diameter than those of the second instars, and they are once again capable of good image formation (Fig. 3d, e, green lines). To evaluate when and how image positions shift over these developmental time points, we established image contrast curves for each of our samples. We then used the values for the two contrast peaks to analyze these data statistically. Our measurements showed that in both eyes the positions of the best images dramatically shift away from the lens during the transition between the second and third instar phase.

Eye 1

The most dramatic shift in focal planes took place between the last second instar, and the first measured third, instar. In eye 1, between these sample points, focal length one increased on average by 78 μm (22 %; from 359 to 437 μm), and focal plane two increased by 138 μm (32 %; from 425 to 563 μm). For both focal planes an ANOVA and further post hoc Tukey tests showed that there was no significant difference in focal length within the second or third instar samples. However, all third instar time points differed significantly from all second instar points (focal plane one: $P \leq 0.0055$ and focal plane two: $P \leq 0.0008$; Fig. 4a, b).

Eye 2

In eye two as well, the most dramatic shifts in focal planes took place between the last second instar sample, and the sample immediately post-molt. In eye two, between these points, focal length one increased on average by 66 μm (from 302 to 368 μm), and focal plane two increased by 104 μm (from 357 to 461 μm). For both focal planes, an ANOVA and further post hoc Tukey tests showed that there was no significant difference in focal length within the second or third instar samples. However, all third instar time points differed significantly from all second instar points ($P < 0.0001$; Fig. 4c, d).

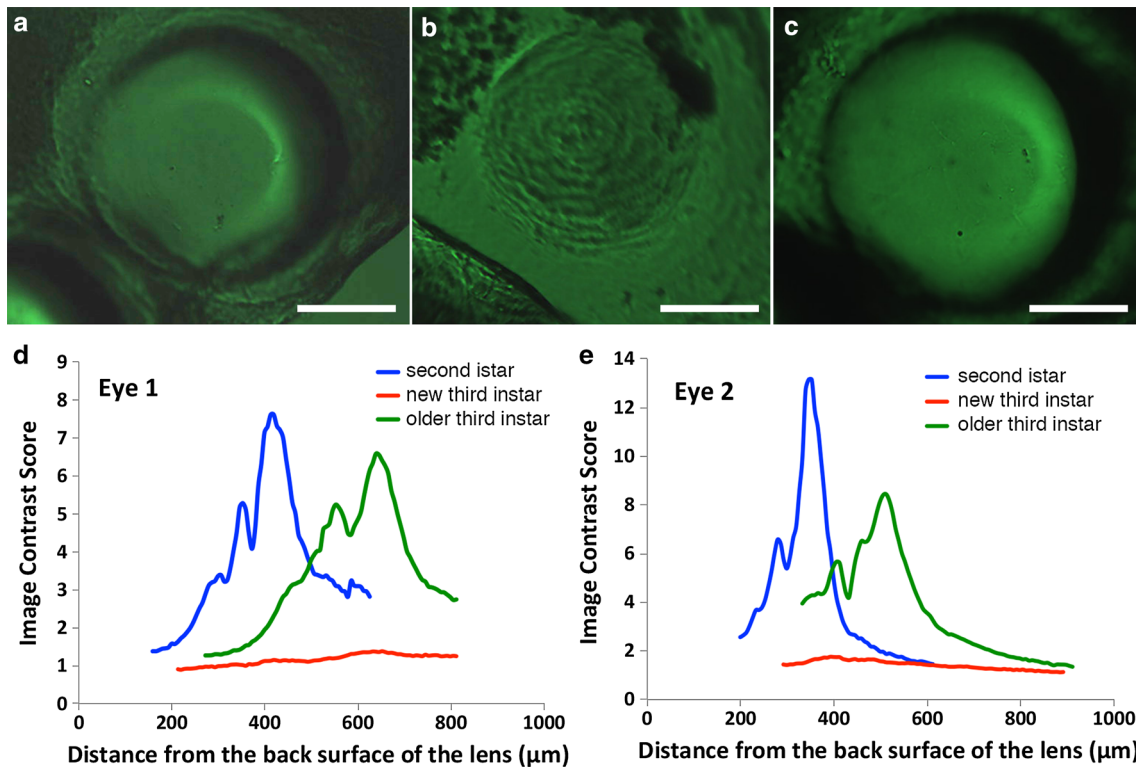


Fig. 3 Reformation of the lens during the transition between second and third instars. **a** The back surface of lenses that are isolated from second instar individuals appears smooth. **b** However, the back surface of lenses that are isolated from freshly molted third instar individuals appears rough and uneven. **c** The back surface of older third instar individuals has recovered its smooth surface. **d** Examples of the image contrast that results from imaging an object through isolated insect lenses from Eye 1. Second and late third instar lenses

show the typical *Thermonectus* bifocal profile, with two *high-contrast peaks*. However, as exemplified by one lens (in red), lenses from newly molted third instar individuals are incapable of producing sharp images, and accordingly no sharp peaks are visible in the image contrast score plot. **e** Example traces from eye two lenses show the same general trend, with bifocal lenses at second and late third instar stages, but non-focusing lenses immediately post-molt. Scale bars 100 µm

Optical and retina fit

To determine how tightly the positions of images that are produced by the lens optics match with the physical distance of the retina, we contrasted selected focal planes with selected anatomical features, as established by Stowasser and Buschbeck (2014). Figure 5a, b illustrates a close match between the length of the crystalline cone, and the back-focal distance of the first focal plane for eye one and two, respectively. This association is apparent in second instar individuals, and then again for third instar larvae that are 8 h old or older. Similarly, the relative position of the second focal plane and the crystalline cone plus distal retina is re-established after molting (Fig. 5c, d).

Discussion

We here provide the first optical analysis of invertebrate camera-type eye growth in rapidly growing insect larvae. Our investigation focused on the transition between second

and third instars. Based on our histological and optical investigations, we conclude that these larvae’s eyes rapidly return to a functionally similar state after molting. Specifically, we found that the eye tubes expand extremely rapidly, as they already took on approximately final length at the earliest post-molt time measured. Lenses transform more slowly, and they are unable to produce images immediately after molting, but they reform sharp, bifocal images by 8 h.

A comparative view on eye growth

Thermonectus eye tube growth is extremely rapid compared to the development of postnatal vertebrate eyes, many of which begin in some state of ametropia, growing and changing at different rates and in particular regions of the eye toward emmetropia. In humans, the overall eye length (axial length) grows about 25 % during the first 3 years of life, and then by about 1 % yearly for the following 10 years (Sorsby and Leary 1969; Larsen 1971; Gordon and Donzis 1985). Which areas of the eye experience the greatest growth differs among species. In several species,

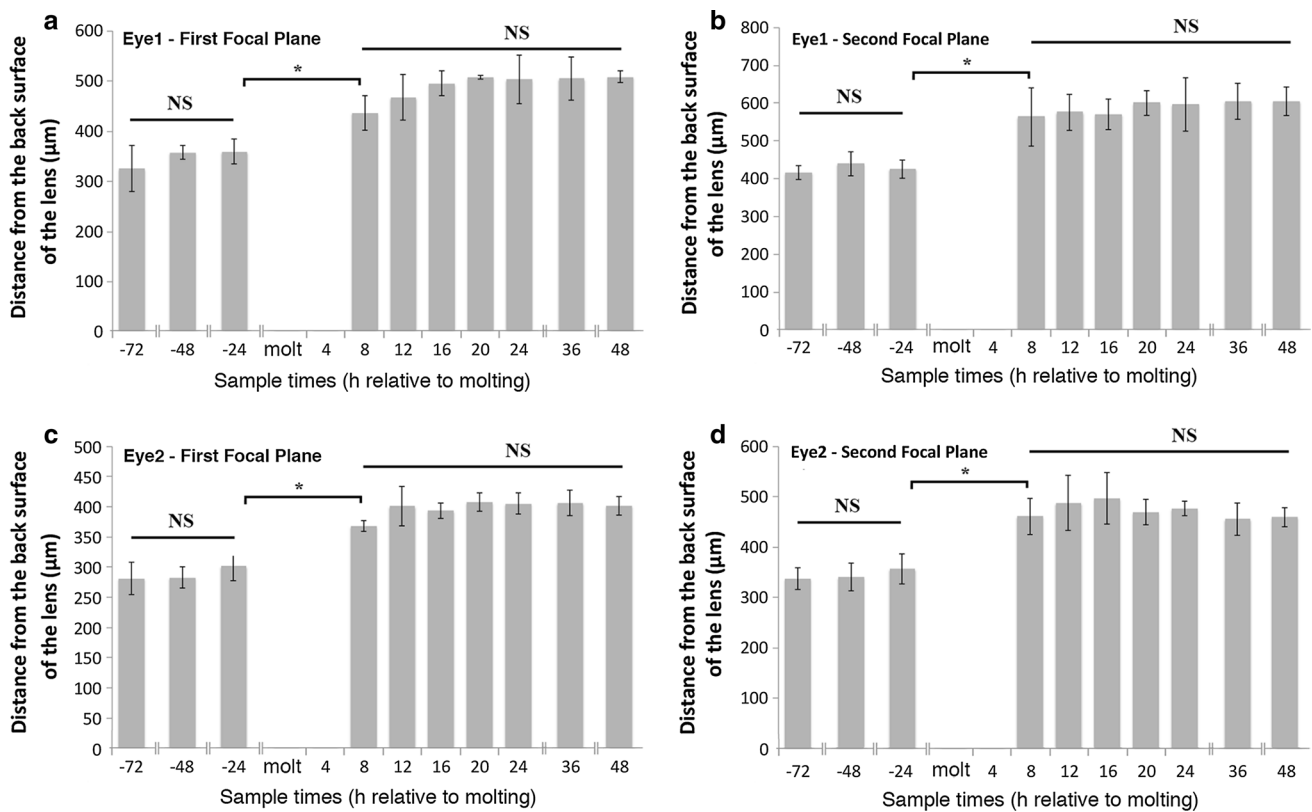


Fig. 4 Shifts in lens optics correlate with the transition between larval stages. **a** Optical measurements of the back-focal distance of the first focal plane of eye one from 3 days prior to the predicted molting time (-72 h) to 2 days post-molt (48 h) show that changes of the lens optics correlate with the two larval stages. As lenses recover their ability to produce images by 8 h post-molt, the position of these

images has shifted away from the lens, and no significant additional shifts are observed within the sampled third instar stages. The same general pattern also holds for the first focal plane of eye 2 (**b**) and for the second focal plane of eye 2 (**c**, **d**, respectively). All graphs illustrate averages and standard deviations

most of the growth is due to the expansion of the vitreous body. For example in guinea pigs the vitreous chamber depth (analogous to the crystalline cone in our investigated species) grew an average of $10 \mu\text{m}$ a day over the course of day 2–30 after birth (Howlett and McFadden 2007). Adult eyes of marmosets have an axial length of ~ 11 mm (Troilo et al. 1993). In one study of this species, axial length increased from an average of ~ 7.75 to 10.5 mm (Graham and Judge 1999) with vitreous chamber growth contributing roughly 90 % to the overall growth of the eye. However, the vitreous chamber is not always an area of rapid growth. For example, in a study on mice, the lens grew particularly strongly while the vitreous chamber depth actually decreased as animals grew (Schmucker and Schaeffel 2004).

Much less is known about eye growth in invertebrates, but there have been a few studies that addressed selected issues that relate to eye growth. For example, isopods have compound eyes that grow post-embryonically, and their growth includes an increase in dioptric apparatus and retina thickness (Keskinen et al. 2002). A study of molting blue

crabs suggests that the visual acuity is reduced around the molting time (Baldwin and Johnsen 2011). Other studies have focused on physiological changes. For example, it has been demonstrated that the sensitivity of photoreceptors markedly increases through post-embryonic development in stick insects (Frolov et al. 2012). In other arthropods, such as mantis shrimp, spectral changes in photosensitivity have been noted (Feller et al. 2015). These arthropods, however, have anatomically distinct larval eyes that transiently work in tandem with the newly forming adult eye, but consequently tend to degenerate, so some of the changes are due to the transition between eyes rather than changes within eyes. In regard to morphological changes, it has been noted that in the assassin bug *Triatoma infestans* an ocular pupil changes size within days following ecdysis (Insausti and Lazzari 2000), but it is unclear to what extent these changes have functional implications. Similarly, post-ecdysis changes have been observed in the spider *Cupiennius salei*, where the lens thickness increases post-ecdysis (Fenk et al. 2010). Here too it is unclear if and how these morphological changes manifest themselves as optical

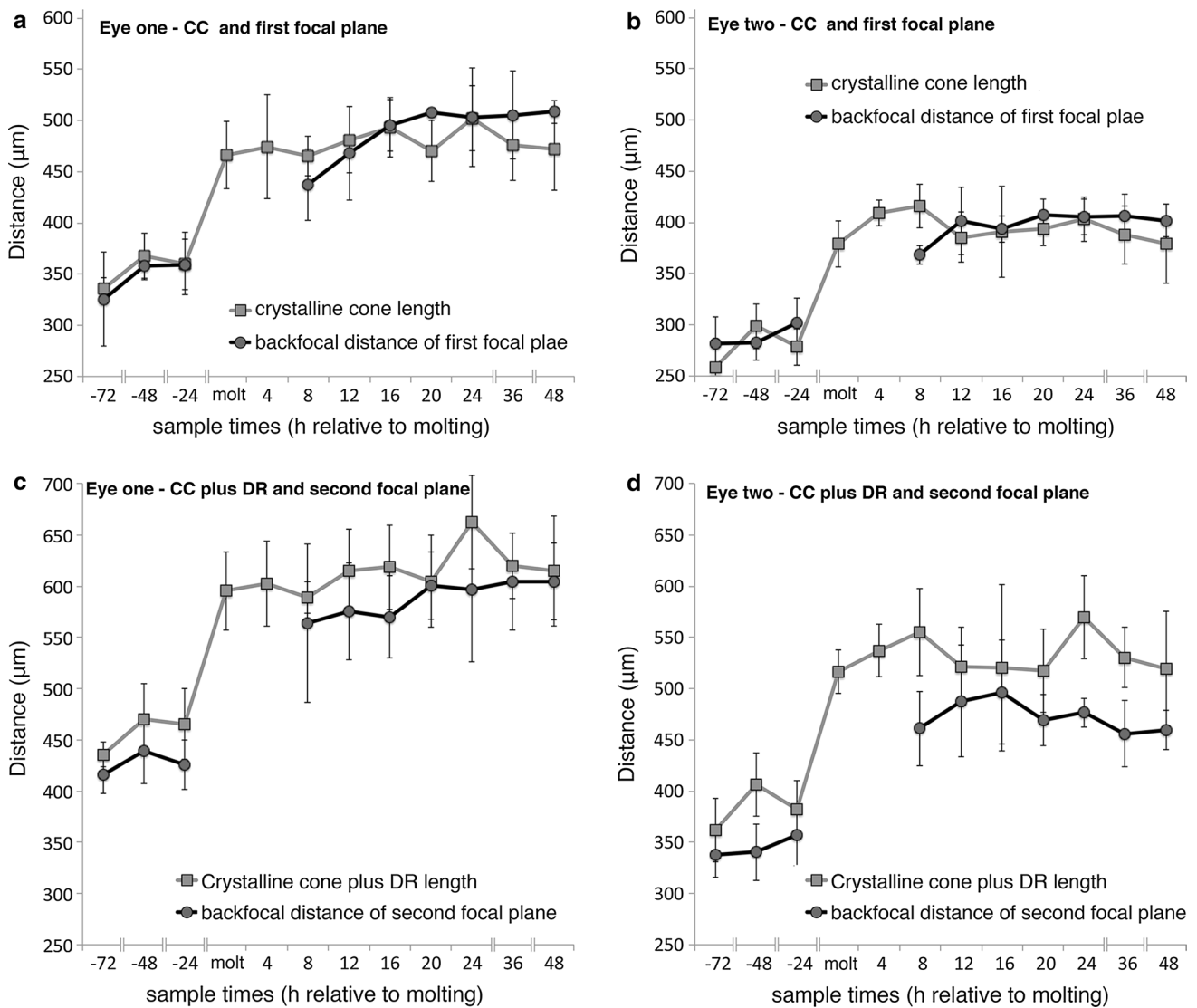


Fig. 5 Histological and optical parameters match similarly in second and in third instar larvae. **a** Based on a previous study on *Thermonectus marmoratus* larvae (Stowasser and Buschbeck 2014), the first focused image is focused below the crystalline cone. Our combined data for eye one shows that this is the case in second instar larvae, and then again as the lens becomes functional in third instar larvae. **b** In eye two as well the crystalline cone length coincides well with the position of the first focused image, both in second and in third instar individuals. **c** In eye one, the second focal plane is positioned near the transition between distal and proximal retinas. Note that optical

measurements were performed with green light, but the proximal retina is UV sensitive, so a slight shift of the actual position is expected due to chromatic aberration. Most importantly though, the relative match between these optical and histological parameters is re-established in third instars by 8 h post-molt. **d** Eye two presents as more myopic, with the second focal plane being located closer to the lens than the distal retina. As is the case for eye one, the relative position of optical and histological parameters is re-established by 8 h post-molt. All graphs illustrate averages and standard deviations

changes, and to date we have found no other studies that address the question of whether and how relative focus is maintained or re-established within rapidly growing arthropod eyes.

In the current study, we find that the eye tubes of *T. marmoratus* expand extremely rapidly, and that their expansion to approximately final length by far precedes optical changes in the lens. The greatest contributor to overall growth was the crystalline cone region, just like the

vitreous does in many vertebrates. Looking at the overall averages between the two instars, it contributed 66 % of the overall eye tube growth in eye one, and 64 % in eye two. The distal retina meanwhile only contributed 18 and 19 %, and the proximal retina only 8 and 3 %, respectively. In part, this is due to the crystalline cone being the largest of these structures, but even proportionally the retinas grew less than the crystalline cone. Specifically, the crystalline cone grew 35 % in Eye 1 and 41 % in Eye 2 compared to

the distal retina which grew 33 and 32 %, and the proximal retina which only grew 13 and 5 %, respectively. It remains unclear why the proximal retina grows least, but it is conceivable that this UV sensitive layer is already close to optimized for maximal photon capture in the smaller eyes of early instars, with little benefit from additional growth in larger eyes. Still the overall growth of the eye tubes corresponded well with gross morphological changes. For comparison, the distance between the eyes expanded by ~34 % between second and third instar individuals.

Compared to the lengthening of the eye tubes, the reformation of the lens is relatively slower, but still, the enlarged lens is fully functional already 8 h post-molt. Based on our observations, a portion of the old lens tends to shed with the old exoskeleton, and our data demonstrate that during the transition to third instars the bi-convex lens expands both in diameter and thickness. These data are in good agreement with our preliminary behavioral observations that indicate that third instar larvae on their first day hunt only about half as many mosquitoes as they do on days 3–5. In fact our behavioral observations indicate a reduced feeding rate even on their second day, leading to the question of how fully proper focusing has been achieved by that time. The good agreement of optical and histological parameters already 8 h post-molt suggests that these eyes well may have achieved proper focusing already at that point. However, the variability in the data leaves room for minor adjustments at later time periods, which need to be investigated further with more sensitive techniques.

Rapid transition opens the possibility for dynamic changes

While there could be minor fine-tuning of eye length at a later time, we are intrigued that all major changes in eye tube length already had taken place at our first sampling point, which was taken within 60 min of molting. This rapid eye expansion suggests a certain level of pre-determined eye growth, but specific adjustments also could be made at the level of the lens, which takes longer to reform. But how can such fast changes be accomplished? We have observed that larvae swallow water and thus, similar to some crustaceans (Dall and Smith 1978; Mangum 1992; Neufeld and Cameron 1994), seem to take up water as part of their molting process. It is not uncommon for invertebrates to show reduced osmolality post-molting (Wilder et al. 2009) and so it is conceivable that the majority of eye growth takes place passively, following influx of water that occurs at the molting process. This idea could be tested: for example, by exposing larvae to iso- or hypotonic conditions post-molt. Any increase in osmolality then would be expected to result in a reduction of eye tube growth, or could even lead to shrinkage of that structure. In insects,

changes in hydrostatic pressure have also long been associated with the molting process (Cottrell 1962), and in vertebrates there are examples of ocular pressure influencing axial growth (Phillips and McBrien 2004), suggesting the potential for interesting parallels between these systems.

Regardless as to whether or not osmosis or other pressure changes play a role in eye tube expansion, the speed by which adjustments are made leads to the possibility for the existence of more dynamic changes than previously thought. There already is evidence for some dynamic changes that involve the crystalline cone in arthropod eyes. For example, it has been reported in mantis shrimp that the crystalline cone lengthens in the light adapted state when compared to the dark adapted state (Schiff et al. 2007). This change is also accompanied by a change in the thickness of the photoreceptor layer, which shortens during the light adapted state so that the overall thickness of the dioptric apparatus plus retina is maintained. More generally, certain dynamic changes in the photoreceptor position in compound eyes have been documented as retinomotoric (Eckert 1968). For example, in the light adapted state the rhabdom of the eyes of the ant *Camponotus* is 10 μm shorter than it is in its dark adapted state (Menzi 1987). Similar rhabdomeric ultrastructure changes have been observed in several other insects, including hemipterans (Walcott 1971). This rhabdomeric adjustment functions to adjust ommatidia to better cope with light intensity changes. It remains unclear if analogous mechanisms exist to facilitate focus plane changes in image-forming invertebrate eyes. Furthermore, it remains unclear if, as is the case in vertebrates (Troilo and Wallman 1991; Flitcroft 2013), visual input is necessary to fully achieve and maintain proper focusing. While these questions generally remain unanswered in invertebrates, it is clear that the intricate eye organization of *T. marmoratus* larvae represents a good system to investigate the mechanisms of eye growth at a more detailed level.

Acknowledgments We thank Annette Stowasser for allowing us to use her MATLAB code and for her many insightful comments to the manuscript, and more generally the Buschbeck lab group for valuable intellectual and editorial feedback. This work was supported by the National Science Foundation under Grants IOS1050754 and IOS1456757 to EKB.

References

- Baldwin J, Johnsen S (2011) Effects of molting on the visual acuity of the blue crab *Callinectes sapidus*. *J Exp Biol* 214(18):3055–3061. doi:10.1242/jeb.056861
- Buschbeck EK (2014) Escaping compound eye ancestry: the evolution of single-chamber eyes in holometabolous larvae. *J Exp Biol* 217:2818–2824

- Buschbeck EK, Sbita SJ, Morgan RC (2007) Scanning behavior by larvae of the predaceous diving beetle, *Thermonectus marmoratus* (Coleoptera: Dytiscidae) enlarges visual field prior to prey capture. *J Comp Physiol A* 193(9):973–982
- Cottrell CB (1962) The imaginal ecdysis of blowflies. Observations of the hydrostatic mechanisms involved in digging and expansion. *J Exp Biol* 39:431–448
- Dall W, Smith DM (1978) Water uptake at ecdysis in western rock lobster. *J Exp Mar Biol Ecol* 35(2):165–176. doi:10.1016/0022-0981(78)90074-6
- Darwin CH (1859) On the origin of species by means of natural selection. John Murray, London
- Eckert M (1968) Hell-Dunkel-Adaption in aconen Appositionsaugen der Insekten. *Zool Jb Physiol Bd* 74:102–120
- Feller KD, Cohen JH, Cronin TW (2015) Seeing double: visual physiology of double-retina eye ontogeny in stomatopod crustaceans. *J Comp Physiol A* 201(3):331–339. doi:10.1007/s00359-014-0967-2
- Fenk LM, Heidlmayr K, Lindner P, Schmid A (2010) Pupil size in spider eyes is linked to post-ecdysal lens growth. *PLoS One*. doi:10.1371/journal.pone.0015838
- Flitcroft DI (2013) Is myopia a failure of homeostasis? *Exp Eye Res* 114:16–24. doi:10.1016/j.exer.2013.02.008
- Flitcroft DI (2014) Emmetropisation and the aetiology of refractive errors. *Eye* 28(2):169–179. doi:10.1038/eye.2013.276
- Frolov R, Immonen EV, Vahasoyrinki M, Weckstrom M (2012) Postembryonic developmental changes in photoreceptors of the stick insect *Carausius morosus* enhance the shift to an adult nocturnal life-style. *J Neurosci* 32(47):16821–16831. doi:10.1523/jneurosci.2612-12.2012
- Gilbert C (1994) Form and function of stemmata in the larvae of holometabolous insects. *Annu Rev Entomol* 39:323–349
- Gordon RA, Donzis PB (1985) Refractive development of the human eye. *Arch Ophthalmol* 103(6):785–789
- Graham B, Judge SJ (1999) Normal development of refractive state and ocular component dimensions in the marmoset (*Callithrix jacchus*). *Vis Res* 39(2):177–187. doi:10.1016/S0042-6989(98)00188-6
- Hofstetter HW (1969) Emmetropization—biological process or mathematical artifact. *Am J Optom Arch Am Acad Optom* 46(6):447–450
- Howlett MHC, McFadden SA (2007) Emmetropization and schematic eye models in developing pigmented guinea pigs. *Vis Res* 47(9):1178–1190. doi:10.1016/j.visres.2006.12.019
- Hung LF, Crawford MLJ, Smith EL (1995) Spectacle lenses alter eye growth and the refractive status of young monkeys. *Nat Med* 1(8):761–765. doi:10.1038/nm0895-761
- Insausti TC, Lazzari CR (2000) An ocellar “pupil” that does not change with light intensity, but with the insect age in *Triatoma infestans*. *Mem Inst Oswaldo Cruz* 95(5):743–746. doi:10.1590/S0074-02762000000500024
- Keskinen E, Takaku Y, Meyer-Rochow VB, Hariyama T (2002) Postembryonic eye growth in the seashore isopod *Ligia exotica* (Crustacea, Isopoda). *Biol Bull* 202(3):223–231. doi:10.2307/1543472
- Kroger RHH, Wagner HJ (1996) The eye of the blue acara (*Aequidens pulcher*, Cichlidae) grows to compensate for defocus due to chromatic aberration. *J Comp Physiol A* 179(6):837–842
- Land MF (1969) Structure of the retinae of the principal eyes of jumping spiders (Salticidae: Dendryphanatidae) in relation to visual optics. *J Exp Biol* 51:443–470
- Land MF (1985) The morphology and optics of spider eyes. In: Barth FG (ed) *Neurobiology of Arachnids*. Springer, Berlin, pp 53–78
- Land MF, Nilsson DE (2012) *Animal Eyes*, 2nd edn. In: *Animal Eyes*. (Oxford Animal Biology Series)
- Larsen JS (1971) Sagittal growth of the eye. 4. Ultrasonic measurement of axial length of eye from birth to puberty. *Acta Ophthalmol* 49(6):873
- Maksimovic S, Cook TA, Buschbeck EK (2009) Spatial distribution of opsin-encoding mRNAs in the tiered larval retinas of the sunburst diving beetle *Thermonectus marmoratus* (Coleoptera: Dytiscidae). *J Exp Biol* 212(23):3781–3794. doi:10.1242/jeb.031773
- Mandapaka K, Morgan RC, Buschbeck EK (2006) Twenty-eight retinas but only twelve eyes: an anatomical analysis of the larval visual system of the diving beetle *Thermonectus marmoratus* (Coleoptera: Dytiscidae). *J Comp Neurol* 497(2):166–181. doi:10.1002/cne.20974
- Mangum C (1992) Physiological aspects of molting in the blue crab *Callinectes sapidus*. *Am Zool* 32(3):459–469
- Mark HH (1972) Emmetropization—physical aspects of a statistical phenomenon. *Ann Ophthalmol* 4(5):393–401
- McBrien NA, Barnes DA (1984) A review and evaluation of theories of refractive error development. *Ophthalmic Physiol Opt* 4(3):201–213. doi:10.1111/j.1475-1313.1984.tb00357.x
- McFadden SA, Howlett MHC, Mertz JR (2004) Retinoic acid signals the direction of ocular elongation in the guinea pig eye. *Vis Res* 44(7):643–653. doi:10.1016/j.visres.2003.11.002
- Menzi U (1987) Visual adaptations in nocturnal and diurnal ants. *J Comp Physiol A* 160(1):11–21. doi:10.1007/bf00613437
- Neufeld DS, Cameron JN (1994) Mechanism of the net uptake of water in molting blue crabs (*Callinectes sapidus*) acclimated to high and low salinities. *J Exp Biol* 188:11–23
- Oshea M, Adams ME (1981) Pentapeptide (proctolin) associated with an identified neuron. *Science* 213(4507):567–569. doi:10.1126/science.611369
- Phillips JR, McBrien NA (2004) Pressure-induced changes in axial eye length of chick and tree shrew: significance of myofibroblasts in the sclera. *Investig Ophthalmol Vis Sci* 45(3):758–763. doi:10.1167/iovs.03-0732
- Schaeffel F, Glasser A, Howland HC (1988) Accommodation, refractive error and eye growth in chickens. *Vis Res* 28(5):639. doi:10.1016/0042-6989(88)90113-7
- Schiff H, Dore B, Boido M (2007) Morphology of adaptation and morphogenesis in stomatopod eyes. *Ital J Zool* 74(2):123–134. doi:10.1080/11250000701245866
- Schmucker C, Schaeffel F (2004) A paraxial schematic eye model for the growing C57BL/6 mouse. *Vis Res* 44(16):1857–1867. doi:10.1016/j.visres.2004.03.011
- Sorsby A, Leary GA (1969) A longitudinal study of refraction and its components during growth. *Spec Rep Ser* 309:1–41 (**Medical Research Council, Great Britain**)
- Stowasser A, Buschbeck EK (2014) Multitasking in an eye: how the unusual organization of the principal larval eyes of *Thermonectus marmoratus* allows for far and near vision and might aid in depth perception. *J Exp Biol* 217:2509–2516
- Stowasser A, Rapaport A, Layne JE, Morgan RC, Buschbeck EK (2010) Biological bifocal lenses with image separation. *Curr Biol* 20(16):1482–1486. doi:10.1016/j.cub.2010.07.012
- Troilo D (1992) Neonatal eye growth and emmetropisation—a literature review. *Eye* 6:154–160 (**London**)
- Troilo D, Wallman J (1991) The regulation of eye growth and refractive state—an experimental study of emmetropization. *Vis Res* 31(7–8):1237–1250. doi:10.1016/0042-6989(91)90048-a
- Troilo D, Howland HC, Judge SJ (1993) Visual optics and retinal cone topography in the common marmoset (*Callithrix jacchus*). *Vis Res* 33(10):1301–1310. doi:10.1016/0042-6989(93)90038-x
- Walcott B (1971) Cell movement on light adaptation in retina of lethercus (Belostomatidae, Hemiptera). *Z Vgl Physiol* 74(1):1. doi:10.1007/bf00297785

- Wallman J, Winawer J (2004) Homeostasis of eye growth and the question of myopia. *Neuron* 43(4):447–468. doi:[10.1016/j.neuron.2004.08.008](https://doi.org/10.1016/j.neuron.2004.08.008)
- Werner S (2014) Thesis: how do stemmata grow? The pursuit of emmetropia in the face of stepwise growth. OhioLINK Electronic Theses and Dissertations Center, University of Cincinnati
- Wilder MN, Huong DTT, Jasmani S, Jayasankar V, Kaneko T, Aida K, Hatta T, Nemoto S, Wigginton A (2009) Hemolymph osmolality, ion concentrations and calcium in the structural organization of the cuticle of the giant freshwater prawn *Macrobrachium rosenbergii*: changes with the molt cycle. *Aquaculture* 292(1–2):104–110. doi:[10.1016/j.aquaculture.2009.03.034](https://doi.org/10.1016/j.aquaculture.2009.03.034)